

METHODOLOGICAL NOTES PACS numbers: 61.50.Ah, 61.50.Ks, 61.50.Nw, 61.66.Fn, **64.30. – t**, 91.60.Fe

High-pressure behavior of the Fe–S system and composition of the Earth's inner core

Z G Bazhanova, V V Roizen, A R Oganov

DOI: https://doi.org/10.3367/UFNe.2017.03.038079

Contents

Abstract. Using the evolutionary crystal structure prediction algorithm USPEX, we identify the compositions and crystal structures of thermodynamically stable compounds in the Fe–S system at pressures in the range of 100 – 400 GPa. We find that at pressures in the Earth's solid inner core (330 – 364 GPa) two compounds are stable — Fe_2S and FeS. In equilibrium with iron, only Fe_2S can exist in the inner core. Using the equation of state of Fe_2S, we find that, in order to reproduce the density of the inner core by adding sulfur alone, 10.6 – 13.7 mol.% (6.4 – 8.4 wt.%) sulfur is needed. An analogous calculation for silicon (where the only stable compound at inner core pressures is FeSi) reproduces the density of the inner core with 9.0 – 11.8 mol.% (4.8 – 6.3 wt.%) silicon. In both cases, a virtually identical mean atomic mass $\bar{M}$ in the range of 52.6 – 53.3 results for the inner core, which is much higher than $\bar{M} = 49.3$ inferred for the inner core from Birch's law. In the case of oxygen (allowing for the equilibrium coexistence of suboxide Fe_2O with iron under core conditions), the inner core density can be explained by the oxygen content of 13.2 – 17.2 mol.% (4.2 – 5.6 wt.%), which corresponds to $\bar{M}$ between 49.0 and 50.6. Combining our results and previous work, we arrive at four preferred compositional models of the Earth's inner core (in mol.%): (i) 86 % (Fe + Ni) + 14 % C; (ii) 84 % (Fe + Ni) + 16 % O; (iii) 84 % (Fe + Ni) + 7 % S + 9 % H; (iv) 85 % (Fe + Ni) + 6 % Si + 9 % H.

Keywords: crystal structure prediction, *ab initio* calculations, evolutionary algorithms, mineral physics

1. Introduction

Sulfur is one of the likeliest light alloying elements in iron-rich cores of terrestrial planets. In the Earth, the inner core is solid and the outer core is liquid and, according to seismic models, the density of both the inner and, especially, the outer core is several percent lower than the density of pure iron or an iron–nickel alloy at relevant pressures and temperatures [1]. From Birch's law [2], one can deduce that the mean atomic mass in the core is approximately 49.3 [3], compared to 55.85 for pure iron. To explain these differences, one has to allow for approximately 10–20 mol.% of lighter elements — the prime candidates being S, Si, O, C, and H [3]. Earlier, we studied the Fe–C system and concluded that the presence of carbon can explain the density of the inner core [4]; here, we consider the Fe–S system, elucidating the analogous role of light alloying sulfur.

Poirier [3] suggested that sulfur remains a good candidate, since it easily dissolves in iron. Li et al. [5] indicated that the Fe–FeS system exhibits eutectic behavior to at least 25 GPa and supported the view that the Earth's inner core contains a significant amount of sulfur. Chen et al. [6] determined the unit cell parameters of Fe_3S using synchrotron X-ray diffraction techniques and externally heated diamond–anvil cells at pressures up to 42.5 GPa and temperatures up to 900 K. Their data suggest that admixing of ≈ 2.1 at.% (1.2 wt.%) sulfur lowers the density of iron by 1%. They estimated 12.5–20.7 at.% (7.6–13.0 wt.%) S in the outer core, and 2.2–6.2 at.% (1.3–3.7 wt.%) S in the inner core; compared to pure iron, the outer core density becomes 6–10% lower, and the inner core 1–3%.

Z G Bazhanova Lomonosov Moscow State University, Leninskie gory 1, 119991 Moscow, Russian Federation
E-mail: bazhanov@srcc.msu.ru,
V V Roizen Moscow Institute of Physics and Technology (State University), Institutskii per. 9, 141700 Dolgoprudnyi, Moscow region, Russian Federation
E-mail: valmipt@gmail.com
A R Oganov Skolkovo Institute of Science and Technology, ul. Nobelya 3, 143026 Skolkovo, Moscow, Russian Federation;
Moscow Institute of Physics and Technology (State University), Institutskii per. 9, 141700 Dolgoprudnyi, Moscow region, Russian Federation;
Lomonosov Moscow State University, Leninskie gory 1, 119991 Moscow, Russian Federation
E-mail: a.oganov@scoltech.ru

Received 6 February 2017, revised 21 February 2017
Uspekhi Fizicheskikh Nauk **187** (10) 1105 – 1113 (2017)
DOI: https://doi.org/10.3367/UFNr.2017.03.038079
Translated by A R Oganov; edited by A Radzig

Alfè et al. [7] have calculated the chemical potentials of S, O, and Si in liquid and solid iron and, assuming that the solid inner core and liquid outer core are in thermodynamic equilibrium, found that O partitions into the liquid much more strongly than S and Si, and that the presence of O in the core is essential to account for the inner–outer core density jump. Alfè et al. [7] proposed that the inner core contains 8.5 ± 2.5 at.% S and/or Si and 0.2 ± 0.1 at.% O, and the outer core 10 ± 2.5 at.% S and/or Si and 8 ± 2.5 at.% O.

Badro et al. [8] have calculated seismic wave velocities and densities in the Fe–(Ni, C, O, Si, S) system and compared them with seismic properties of the Earth's core. They found that oxygen is required as a major light element in the core, whereas silicon, sulfur, and carbon are not required. They also found that the concentration of silicon in the outer core cannot be higher than 4.5 wt.%, and the concentration of sulfur must be below 2.4 wt.%.

Hirose et al. [9] have reviewed recent experimental and theoretical studies on the high P–T crystal structures of iron–nickel, –silicon, –oxygen, –sulfur, –carbon, and –hydrogen compounds. They reported that, indeed, the inner core might include ~ 6 wt.% S, if sulfur were the sole light alloying component. Moreover, considering the density jump across the inner core boundary, they pointed out that the outer core may include ~ 6 wt.% silicon, ~ 3 wt.% oxygen, and 1–2 wt.% sulfur. Using experimental data on phase equilibria in the Fe–S system at pressures up to 200 GPa, Saxena and Eriksson [10] concluded that the inner core has a maximum temperature of 4428 ($\pm$500) K with a sulfur content of ~ 15 wt.%, but, to be consistent with seismic data, the presence of yet another light element is necessary.

To conclude, the status of sulfur as a candidate light alloying element in the Earth's core is somewhat uncertain. However, the existing evidence for and against sulfur in the core involves many assumptions and extrapolations. Here, we consider the Fe–S system, searching for stable iron sulfides at pressures of the inner core, analyzing their crystal chemistry, and determining, on the basis of the most accurate available data, how much sulfur is needed in order to reproduce the observed density of the Earth's inner core.

Pure iron, sulfur, and FeS have been the subjects of numerous experimental and theoretical studies, and some degree of consistency is beginning to emerge. Akahama et al. [11], using angle-dispersive X-ray diffraction, showed that a base-centered orthorhombic (bco) structure of compressed sulfur is stable above 83 GPa. The experimental results of Luo et al. [12], based on energy-dispersive X-ray diffraction at pressures up to 212 GPa, detected a transition to a new phase at 162 GPa. Its X-ray reflections have been indexed with a simple rhombohedral β-Po structure. Degtyareva et al. [13] studied sulfur up to 160 GPa and found an incommensurately modulated body-centered monoclinic (bcm) structure to be stable at 300 K and pressures between 83 and 153 GPa, above which it transforms into the β-Po structure. Pseudopotential *ab initio* calculations [14] were performed for three high-pressure phases of sulfur (bco, β-Po, and body-centered cubic (bcc)). These calculations did not reproduce the reported bco-to-β-Po phase transition, but showed a transition from β-Po to bcc at ~ 550 GPa. First-principles calculations for sulfur at 200–600 GPa and $T = 0$ K within the local density approximation predicted phase transitions in the sequence β-Po $\rightarrow$ simple cubic (sc) $\rightarrow$ bcc, with the simple cubic structure favored over a wide range of pressures from 280 to 540 GPa [15].

Experimental and theoretical studies of iron at high pressures are numerous and only recently reached a consensus. It was established, both experimentally and theoretically, that the nonmagnetic hcp phase of iron is stable at 13 GPa and room temperature [16–18]. At pressures relevant to the Earth's core (136–330 GPa for the outer core, and 330–364 GPa for the inner core), several new phases have been proposed. For example, a double hexagonal close-packed phase of iron [19] and an orthorhombically distorted hcp structure [20] were reported at high pressures and temperatures; other proposals included a body-centered tetragonal structure and the bcc structure [21, 22]. The proposal of the bcc structure at ultrahigh pressures and temperatures presents an interesting case: there are two bcc phases at atmospheric pressure, one ferromagnetic (at ambient conditions) and one paramagnetic (with disordered local magnetic moments) at high temperatures [23]. In principle, a third, nonmagnetic high-pressure bcc phase is not impossible, but Stixrude and Cohen [24] found that it is dynamically unstable (i.e., possesses soft modes, namely, phonons with imaginary frequencies) at high pressures and zero temperature. Nevertheless, Belonoshko et al. [21] and Vočadlo et al. [25] demonstrated that soft modes in this structure are anharmonically suppressed at temperatures characteristic of the Earth's core. Belonoshko et al. [21] using an embedded-atom potential found this phase to become thermodynamically stable, while Vočadlo et al. [25] used more accurate DFT calculations and found this phase to be slightly less stable than hcp — but this small free energy difference can be overturned by the addition of impurities (Si, S), which may stabilize the bcc phase.

Following these studies, Dubrovinsky et al. [26] also claimed on the basis of their experiments that the (Fe, Ni) alloy adopts the bcc structure at high pressures and temperatures, but experiments of Kuwayama et al. [27] found the opposite. In an experimental *tour de force*, Tateno et al. [28] showed that at actual conditions in the Earth's inner core pure Fe has the hcp structure. Calculations made by Côté, Vočadlo and Brodholt [29] showed that the addition of Ni to iron only further stabilizes the hcp structure over bcc.

Iron sulfide (FeS) exhibits numerous phase transitions at low pressures. Its ultrahigh-pressure behavior was investigated in detail using first-principles calculations up to the pressure of 400 GPa [30], and the transition sequence at 0 K was found to be troilite (FeS I) $\rightarrow$ antiferromagnetic MnP type phase (FeS II) $\rightarrow$ monoclinic phase (FeS III) $\rightarrow$ nonmagnetic MnP type phase (FeS VI) $\rightarrow$ *Pmmn* phase (FeS VII). The *Pmmn* phase with a distorted NaCl-type structure is stable from 135 GPa up to at least 400 GPa. The experimental results by Sata et al. [31] showed that a CsCl-type structure is stable at high temperatures and pressures above 180 GPa, hinting at a possible problem with DFT description of FeS. We address this issue here, too.

2. Methodology

Our calculations are based on the evolutionary crystal structure prediction method USPEX [32–34] and density functional theory [35, 36] within the generalized gradient approximation (GGA) [37]. Such calculations for pure Fe at high pressures [32] have produced the known lowest-enthalpy structure, hcp-Fe, in agreement with available experimental evidence [28]. For pure S, we predicted ground-state struc-

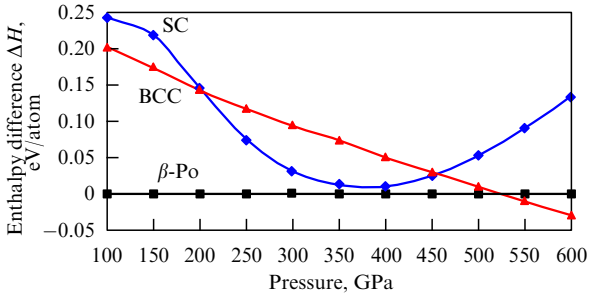

Figure 1. High-pressure stability of sulfur allotropes at $T = 0$ K.

tures by USPEX: the β-Po structure in the pressure range of 100–540 GPa, and bcc for > 540 GPa.

From Fig. 1, one can see a direct phase transition of S from β-Po to bcc, bypassing the simple cubic structure, as in Ref. [14], and questioning the existence of the simple cubic structure predicted in Ref. [15]. It should be noted, however, that at pressures around 350–400 GPa this phase is competitive with the β-Po phase (Fig. 1). Figure 2 shows a comparison between theoretical (at 0 K) and experimental equations of state of pure sulfur [11–13], iron [38–41], and FeS [42]. Good agreement can be seen between theory and experiment.

First, we performed variable-composition evolutionary searches for stable compounds/structures in the Fe–S system at pressures of 300 GPa and 400 GPa, followed by detailed fixed-composition evolutionary searches at 300 GPa and 400 GPa for the most promising compositions (FeS, Fe_2S, FeS_2, Fe_3S, FeS_3, Fe_3S_2, Fe_5S_2, and Fe_9S_5). These searches were performed for FeS with 8 and 16 atoms per cell, for Fe_2S with 6, 9, 12, and 16 atoms per cell, for FeS_2 with 6, 9, 12, 15, and 18 atoms per cell, for Fe_3S with 8, 12, and 16 atoms per cell, for FeS_3 with 4 and 8 atoms per cell, for Fe_3S_2 with 10, 15, and 20 atoms per cell, and for Fe_5S_2 and Fe_9S_5 with 14 atoms per cell.

A typical USPEX simulation included 30–40 structures per generation for fixed-composition runs (for variable-composition runs, the initial population included 150 structures, and all subsequent generations had 60 structures), the lowest-enthalpy 60% of which were used for producing the next generation of structures (70% of the offspring produced by heredity, 10% by atomic permutation or transmutation, and 20% by lattice mutation). All structures produced by USPEX were relaxed using the GGA functional [37] and projector-augmented wave (PAW) method [43, 44], as implemented in the VASP code [45]. We used PAW potentials with an [Ar] core (radius 2.3 a.u.) and [Ne] core (radius 1.9 a.u.) for Fe and S atoms, respectively, and a plane wave kinetic energy cut-off of 600 eV. Structure relaxations done within USPEX simulations employed homogeneous Γ-centered meshes with a reciprocal-space resolution of $2\pi \times 0.03$ Å^{-1} and Methfessel–Paxton electronic smearing [46] with $\sigma = 0.07$ eV. Having identified several lowest-enthalpy structures using USPEX, we carefully re-relaxed them and recalculated their enthalpies using the tetrahedron method with Blöchl corrections [47]. To assess the possible magnitude of electron correlation effects on phase stability, we compared results of GGA and GGA+U calculations, the latter being based on Dudarev's formulation of the DFT+U method [48].

The thermodynamic stability of compounds in the Fe–S system was determined using the thermodynamic convex hull

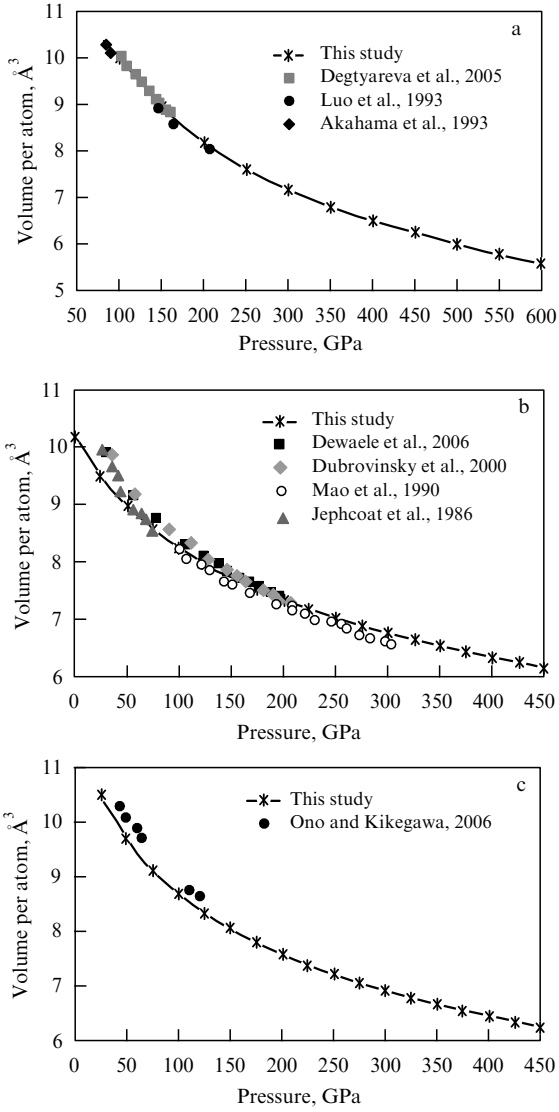

Figure 2. Comparison of the theoretical ($T = 0$ K) and experimental ($T = 300$ K) equations of state: (a) sulfur (experiments: Akahama et al. [11], Luo et al. [12], Degtyareva et al. [13]); (b) iron (experiments: Dewaele et al. [38], Dubrovinsky et al. [39], Mao et al. [40], Jephcoat et al. [41]), and (c) FeS (experiments: Ono and Kikegawa [42]).

construction: put plainly, a compound is stable when it has lower free energy than any isochemical mixture of any other compounds. After thermodynamically stable phases were identified, we computed their phonons to check their dynamical stability. Phonons and the thermodynamic properties of Fe–S compounds were calculated using the finite-displacement approach as implemented in the PHONOPY code [49, 50]. To perform phonon calculations, all structures were fully relaxed until all force components became less than 0.01 meV Å^{-1} in absolute value. We constructed then supercells (typically $2 \times 2 \times 2$, with side lengths of more than 10 Å) and displaced atoms by 0.01 Å to get the forces, which were then used to construct the force constants matrix. The dynamical matrix was next constructed and diagonalized at a very dense reciprocal-space mesh.

To clarify the details of iron sulfide (FeS) high-pressure phase transitions, we constructed the phase diagram in (P, T)-coordinates. For this purpose, we computed Gibbs free energies G of the relevant FeS phases using the

quasiharmonic approximation:

$$G(P,T) = E_0(V) + F_{\text{vib}}(T,V) + P(T,V)\,V, \tag{1}$$

where E_0 is the total energy from DFT calculations, and F_{vib} is the vibrational Helmholtz free energy calculated from the relationship

$$F_{\text{vib}}(T,V) = k_{\text{B}}T\int g\big(\omega(V)\big)\,\ln\left[1-\exp\left(-\frac{\hbar\omega(V)}{k_{\text{B}}T}\right)\right]\mathrm{d}\omega + \frac{1}{2}\int g\big(\omega(V)\big)\,\hbar\omega\,\mathrm{d}\omega\,, \tag{2}$$

and the pressure is given by

$$P(T,V) = -\frac{\partial\big(E_0(V)+F_{\text{vib}}(T,V)\big)}{\partial V}\,. \tag{3}$$

Here, $g(\omega(V))$ is the phonon density of states at the given volume. Equations of state were fitted using the 3rd-order Birch–Murnaghan equation of state [51]. By calculating the differences between Gibbs free energies, we were able to construct the FeS phase diagram.

3. Results

3.1 Structures and compositions of stable iron sulfides at ultrahigh pressures

Our predicted convex hulls at various pressures and the phase diagram of the Fe–S system are shown in Fig. 3. In the pressure range studied here, only three compounds have stability fields: FeS_2, FeS, and Fe_2S. Crystal structures of the new stable phases predicted by USPEX are given in Table 1. In the entire pressure ranges of their stability (Fig. 3b), the predicted phases are dynamically stable (Fig. 4).

In the whole pressure range studied here, Fe_2S possesses only one stable structure, which has the *Pnma* space group and S atoms coordinated by ten Fe atoms in an irregular coordination. Geometrically, this is not a close-packed structure (Fig. 5a); nevertheless, its physical density is very high. Each Fe atom is coordinated by five S and eight Fe atoms.

Table 1. Structural parameters of some of the phases found by USPEX. *Pmmn*-FeS is the same phase as previously predicted by us (Ono et al. [30]) and confirmed here again.

Phase (space group), pressure, unit cell parameters	Wyckoff position		*x*	*y*	*z*
FeS (*Pmmn*), 300 GPa, $a = 3.629$ Å, $b = 2.296$ Å, $c = 3.317$ Å	Fe	2a	0.75	0.75	0.8619
	S	2b	0.25	0.75	0.6358
Fe_2S (*Pnma*), 300 GPa, $a = 4.234$ Å, $b = 3.178$ Å, $c = 5.984$ Å	Fe	4c	0.6665	0.25	0.4304
	Fe	4c	0.4687	0.75	0.2053
	S	4c	0.7885	0.75	0.6052
FeS_2 (*C*2/*m*), 400 GPa, $a = 6.582$ Å, $b = 3.624$ Å, $c = 3.766$ Å, $\beta = 118.41°$	Fe	4i	0.6338	0.5	0.4027
	S	4i	0.5331	0	0.2798
	S	4i	0.7996	0	0.0332

In the pressure range investigated here (100–400 GPa), FeS has two stable phases: *Pnma* (the well-known MnP type structure, a distortion of the NiAs type structure) stable below 122 GPa, and *Pmmn*, which is stable above 122 GPa. The structure of the *Pmmn*-phase (Fig. 5b) can be described as a strongly distorted NaCl-type structure, with well-defined close-packed layers of Fe and S atoms.

In the same pressure range, FeS_2 exhibits two stable phases: the well-known $Pa\bar{3}$ (pyrite) predicted to be stable at pressures below 188 GPa, and *C*2/*m* stable above 188 GPa. The remarkable structure of *C*2/*m*-FeS_2 (Fig. 5c) has a diamond-like Fe sublattice (each Fe is surrounded by four other Fe atoms and six S atoms). Each S has three neighboring Fe atoms and three neighboring S atoms. At low temperatures and low pressures (below 6 GPa according to the experiment by Parthasarathy [52], and below 3.7 GPa according to GGA calculations by Gudelli [53]), another polymorph, marcasite (space group *Pnnm*), is stable.

In high-pressure high-temperature experiments, the following phases of FeS have been observed: *Pnma* at pressures up to at least 120 GPa [42], and CsCl-type (space group $Pm\bar{3}m$) at pressures above 180 GPa [31]. Our calculations (Fig. 6) show the *Pnma* → *Pmmn* phase transition at 122 GPa (GGA) or 192 GPa (GGA+*U*, with $U = 4$ eV), and both with and without the *U*-correction, the CsCl-type phase is always

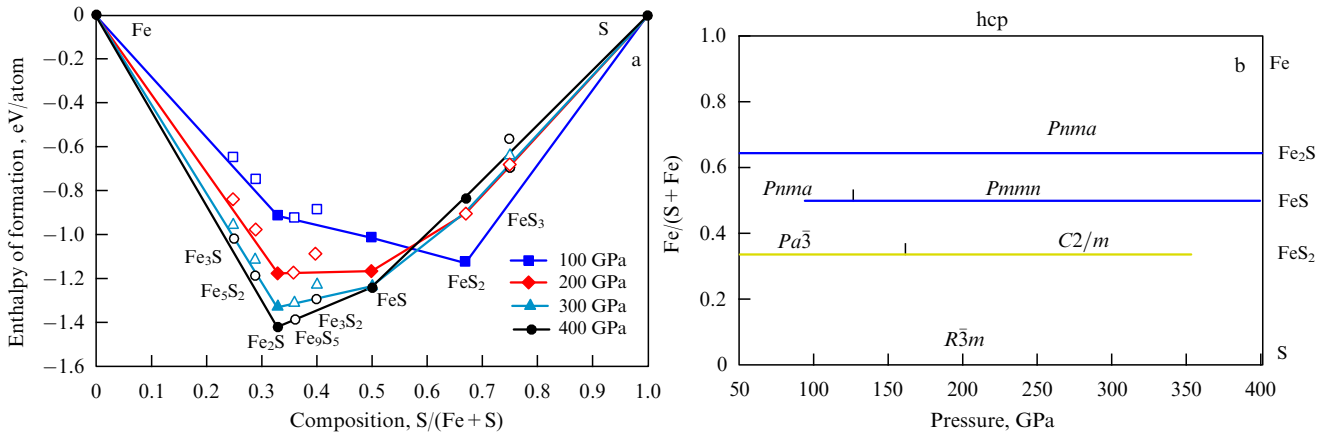

Figure 3. (Color online.) Thermodynamics of the Fe–S system: (a) convex hulls at different pressures and zero temperature, and (b) composition–pressure phase diagram ($T = 0$ K).

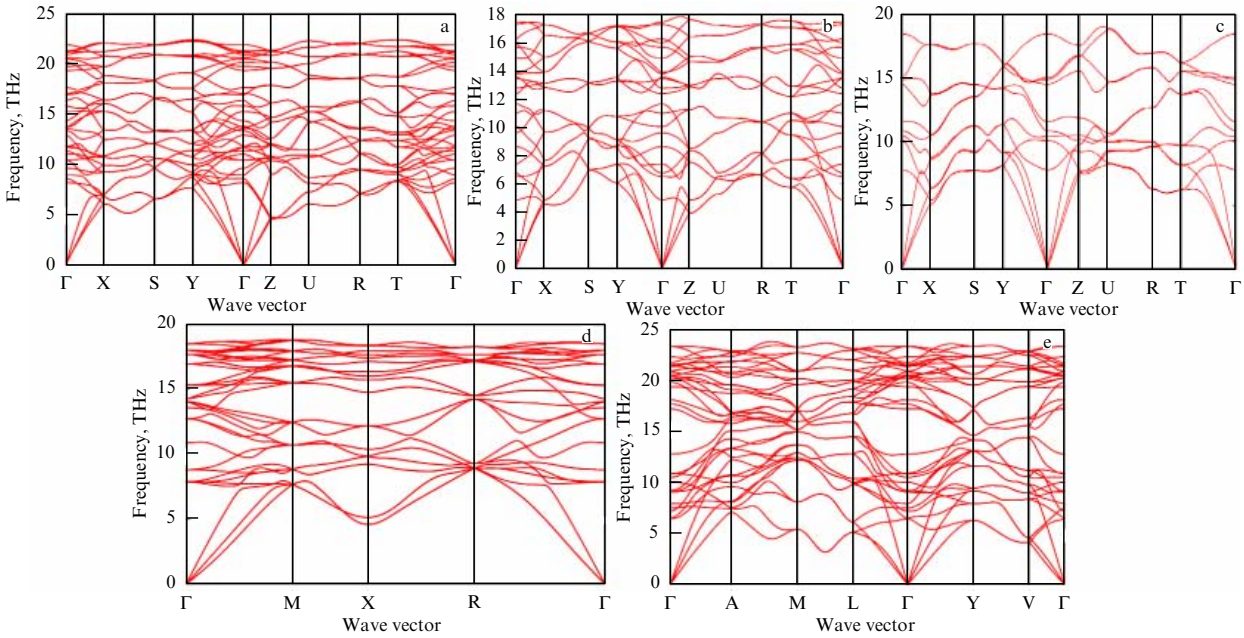

Figure 4. Phonon dispersion curves of (a) *Pnma*-Fe_2S at 200 GPa , (b) *Pnma*-FeS at 80 GPa, (c) *Pmmn*-FeS at 100 GPa, (d) $Pa\bar{3}$-FeS_2 at 75 GPa, and (e) $C2/m$-FeS_2 at 250 GPa.

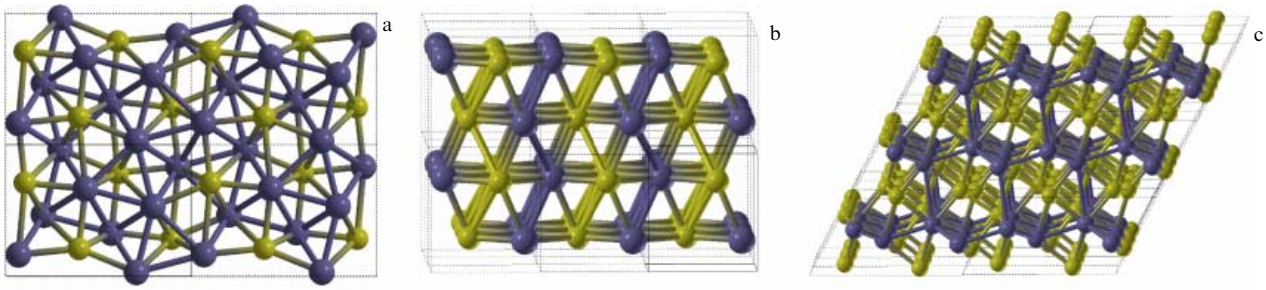

Figure 5. (Color online.) Structures of thermodynamically stable high-pressure iron sulfides found in this work: (a) Fe_2S (*Pnma*), (b) FeS (*Pmmn*), and (c) FeS_2 ($C2/m$). Purple balls — iron atoms, and yellow balls — sulfur atoms.

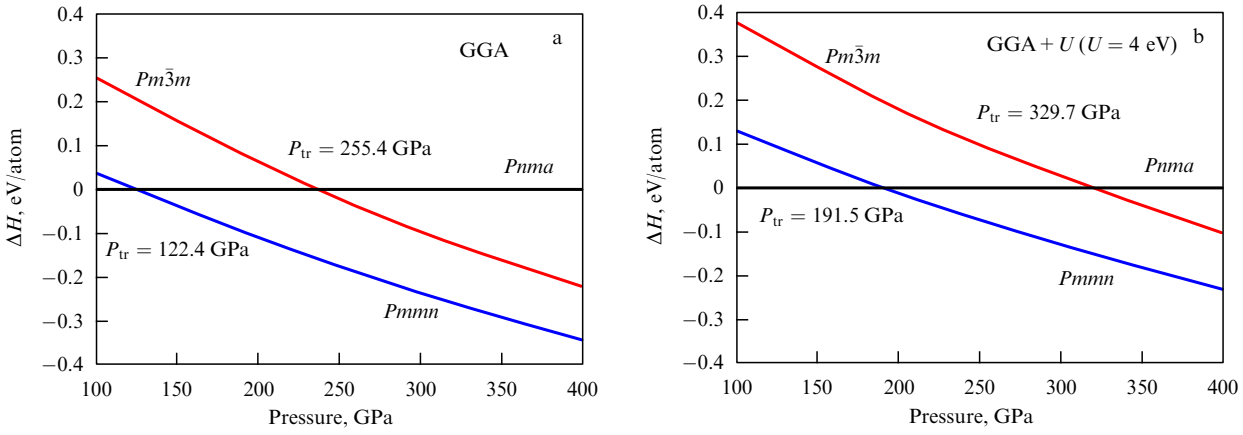

Figure 6. Enthalpy differences between various FeS phases: (a) GGA calculations, and (b) GGA+U ($U = 4$ eV) results at $T = 0$ K.

metastable at zero temperature (by 0.1–0.15 eV/atom, which can be overturned by thermal effects; see below). The difference between GGA and GGA+U results with such a large value of U gives an upper bound of the effects of electron correlation, because these effects are strongly reduced in metallic materials, such as FeS phases.

The CsCl-type phase, observed in experiment, is most likely stabilized by temperature. We have computed the high-pressure phase diagram of FeS based on GGA calculations and the quasiharmonic approximation (Fig. 7). We see indeed that the CsCl-type phase may have a stability field at high temperatures. Experimental points where this phase was

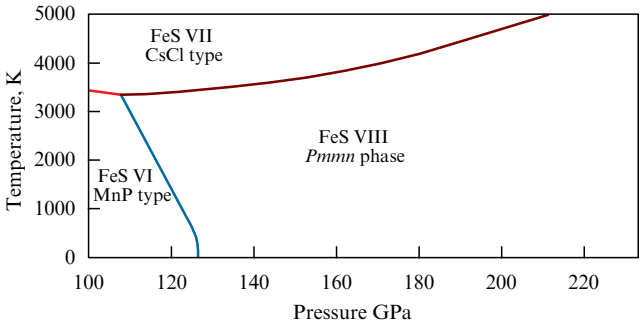

Figure 7. Phase diagram of FeS obtained in the quasiharmonic approximation.

found (186–270 GPa, 298–1300 K) [31] fall within the computed stability field of the *Pmmn* phase, but even a moderate change in thermodynamic properties (to compensate for the errors of the GGA and of the quasiharmonic approximation) of phases can extend the stability field of the CsCl-type phase to include these (P, T)-conditions.

The *Pmmn* structure of FeS predicted in Ref. [30] is quite remarkable due to its unexpected relationship with another known polymorph of FeS — mackinawite. We found (see Fig. 8) that upon decompression to 20 GPa our *Pmmn* structure spontaneously, i.e., without any activation barrier, transforms into a distorted mackinawite structure (space group *Pmmn*), which becomes ideal (undistorted) mackinawite (space group $P4/nmm$) at 15 GPa. This metastable transition is barrierless and first-order one, and has an 11.3% density jump. The mechanism of the mackinawite–*Pmmn* transition involves the collapse and distortion of tetragonal mackinawite layers and the formation of interlayer bonds. This structural relationship implies that *Pmmn*-FeS can be made relatively easily by compression of mackinawite.

At zero pressure, mackinawite has theoretical cell parameters $a = b = 3.596$ Å and $c = 5.794$ Å; experimental values are $a = b = 3.674$ Å and $c = 5.033$ Å [54]: one can see good agreement for $a = b$ parameters, while there is a significant discrepancy for the c-parameter due to the neglect of van der Waals interactions at the GGA level of theory. Indeed, the

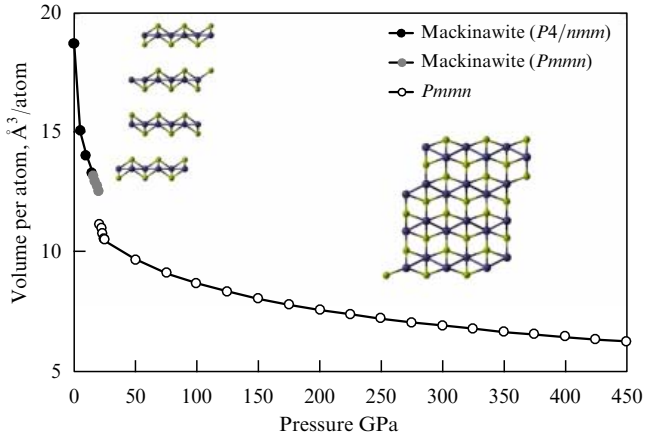

Figure 8. (Color online.) Decompression behavior of the predicted *Pmmn* phase of FeS at zero temperature, showing a spontaneous transition to mackinawite (GGA results).

Table 2. Experimental [54] and theoretical (this study) lattice parameters of mackinawite at 0 GPa.

	a	b	c
Experiment	3.674	3.674	5.033
GGA	3.596	3.596	5.794
GGA + D2	3.562	3.562	4.900
GGA + TS	3.570	3.570	5.074
opt-PBE-vdW	3.602	3.602	5.026

c-parameter corresponds to the interlayer distance, entirely determined by the van der Waals (vdW) interactions. We conducted relaxation of the mackinawite structure using two methods including vdW correction: the D2 method of Grimme (DFT-D2 [55]), and the Tkatchenko–Scheffler method (DFT-TS [56]). In addition, we tested the vdW-DF correlation functional of Langreth and Lundqvist et al. [57–61] together with the opt-PBE exchange-correlation functional which was optimized for use with the vdW-DF functional. Experimental and theoretical lattice parameters of mackinawite are presented in Table 2. It can be noticed that, in particular, the results of the opt-PBE-vdW method are in excellent agreement with experimental data.

3.2 How much sulfur is needed to explain the density of the inner core?

Parameters of the predicted static equations of state describing Fe–S phases are given in Table 3. Using the computed equations of state, we determined the molar concentration of sulfur needed to explain the density of the inner core by matching the observed density of the inner core to the density of the mixture of hcp-Fe and the stable sulfide Fe_2S. We also tried FeS, although this compound is unlikely to be present at realistic concentrations of sulfur in the inner core. Such calculations are important for estimating the robustness of our matching concentrations, i.e., their independence of the chosen reference phase. For comparison and for completeness, we also computed the matching concentration of silicon using previous calculations for the Fe–Si [62] and Fe–O systems [63] (see Table 4).

These estimates give the concentration needed to match the inner core density, if sulfur (or silicon) were the only light alloying element, and, since several alloying elements are likely to be present in different concentrations, give the upper bound for the concentration of each element. Such a procedure for calculating the molar concentration of the light element for Fe–C and Fe–H alloys was carried out in our earlier paper [4]. It is crucial to incorporate the temperature

Table 3. Theoretical third-order Birch–Murnaghan equations of state of the nonmagnetic high-pressure phases in Fe–S systems.

Phase	V_0, Å^3/atom	K_0, GPa	K_0'
hcp-Fe	10.16	303.37	4.31
Pmmn-FeS*	11.71	170.02	4.50
Pnma-Fe_2S	10.69	210.11	4.74
$C2/m$-FeS_2	13.51	104.05	4.56
$Pm\bar{3}m$-FeSi	10.46	256.0	4.25
$R\bar{3}m$-S	17.11	66.71	3.82

* Parameters of the 3rd-order Birch–Murnaghan equation of state in the pressure interval of 25–450 GPa. Results are very close to the published theoretical values (Ono et al. [30]): $V_0 = 11.74$ Å^3/atom, $K_0 = 176.0$ GPa, $K_0' = 4.35$, where K_0 — bulk modulus at zero pressure, and K_0' — its pressure derivative.

Table 4. Estimated matching concentrations of sulfur, silicon, carbon, hydrogen, and oxygen based on reference stable binary compounds FeS, Fe_2S, FeSi, Fe_2C, FeH, and Fe_2O at inner core conditions.

Fe–X	x, mol.%	x, wt.%	$\bar{M}$
Pmmn-FeS	9.5–12.4	5.7–7.5	52.9–53.6
Pnma-Fe_2S	10.6–13.7	6.4–8.4	52.6–53.3
$Pm\bar{3}m$-FeSi	9.0–11.8	4.8–6.3	52.6–53.3
Pnma-Fe_2C	11.2–14.6	2.6–3.6	49.4–50.9
$Fm\bar{3}m$-FeH	16.9–22.0	0.4–0.5	43.8–46.6
$I4/mmm$-Fe_2O	13.2–17.2	4.2–5.6	49.0–50.6

effects, for which we employed the formula

$$\rho_{\rm IC} = \rho^T_{\rm Fe} + \frac{\partial\rho}{\partial x}\,x \Rightarrow \rho_{\rm IC} - \rho^T_{\rm Fe} = \frac{\rho^0_{\rm Fe_2S} - \rho^0_{\rm Fe}}{0.33}\,x\,, \qquad (4)$$

where $\rho_{\rm IC}$ is the PREM (preliminary reference Earth model) [64] density of the inner core at a given depth, $\rho^T_{\rm Fe}$ is the density of pure iron at a given temperature [38], and $\rho^0_{\rm Fe}$ and $\rho^0_{\rm Fe_2S}$ are the computed zero-temperature densities of Fe and Fe_2S. The number 0.33 in the right-hand side of Eqn (4) indicates the molar fraction of sulfur in Fe_2S. The resulting concentrations for the Fe–S and similarly made estimates for the Fe–Si and Fe–O systems (from this study) and Fe–C and Fe–H alloys (from Bazhanova et al. [4]), estimated along isotherms 5000 K and 6000 K are given in Table 4.

Three conditions must be met if a certain element (S, Si, O, C, or H) is to be considered as the main light element in the core:

(i) the concentration of the light elements needed to explain the observed core density at the expected core temperatures (5000–6000 K [65]) should not be unacceptably large (roughly < 20 mol.%);

(ii) this quantity should not display large and non-monotonic variations with depth, and

(iii) the resulting mean atomic mass $\bar{M}$ should be reasonably close to the one determined from Birch's law [2], i.e., 49.3 [3].

For both Fe–S and Fe–Si systems (Fig. 9), we see moderate variations of the matching concentrations with depth, leading to the average atomic mass $\bar{M} \sim 53$, which is much higher than $\bar{M} = 49.3$ [3] derived for the Earth's core from Birch's law [2]. Neither silicon nor sulfur can be the only light alloying element. Likewise, hydrogen cannot be the only light alloying element either: its matching concentration shows more variation with depth [4] and corresponds to the average atomic mass $\bar{M} = 45$, which is much too low. Carbon and oxygen are the only elements that alone can explain both the density and $\bar{M}$ of the inner core with the composition (in atomic %)

$$86\,\%\,(\mathrm{Fe} + \mathrm{Ni}) + 14\,\%\,\mathrm{C}$$

or

$$84\,\%\,(\mathrm{Fe} + \mathrm{Ni}) + 16\,\%\,\mathrm{O}\,.$$

Oxygen is known to have very low solubility in crystalline iron at pressures and temperatures of the Earth's core [7], but is highly soluble in liquid iron at conditions of the outer core [7] and can form in the inner core a separate phase (e.g., Fe_2O [63]) precipitating from the molten outer core (note, however, that recent experiments cast doubt on the presence of large concentrations of oxygen even in the outer core [66]).

Considering simultaneous presence of two light alloying elements, we found that only two models produced satisfactory results:

$$84\,\%\,(\mathrm{Fe} + \mathrm{Ni}) + 7\,\%\,\mathrm{S} + 9\,\%\,\mathrm{H}\,,$$
$$85\,\%\,(\mathrm{Fe} + \mathrm{Ni}) + 6\,\%\,\mathrm{Si} + 9\,\%\,\mathrm{H}\,.$$

It is remarkable that all these models have a practically identical iron (+nickel) content of $\sim 85\%$. We also note that the last two models can be linearly mixed in any proportion, but not all other models can be combined: it was shown in Refs [67, 68] that hydrogen and carbon cannot coexist in the Earth's core, i.e., they are mutually exclusive. Silicon and oxygen are also mutually exclusive [69]. We do not know whether carbon and oxygen are mutually compatible in the core.

Checking against all the other known properties of the core (compressional and shear seismic wave velocities, Poisson's ratio, density jump at the inner–outer core boundary) is necessary, as it will help to discriminate between the four compositional models found here. It is already known that the carbon-only model, with 86 % (Fe + Ni) + 14% C, explains not only the density and the Birch number of the inner core but, according to recent experiments [70–72], also the compressional and shear wave velocities and the anomalous Poisson ratio of the inner core. Indeed, Chen et al. [71] favored this model and concluded that up to two thirds of the Earth's carbon can be in the Earth's core. Now, the other models need to be tested against these constraints as well.

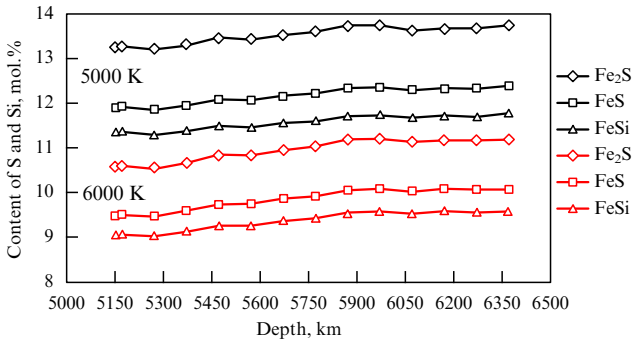

Figure 9. (Color online.) Matching molar concentration of sulfur and silicon as a function of depth in the inner core using equations of state for Fe_2S, FeS, and FeSi. Results are shown along the 5000 K and 6000 K isotherms.

4. Conclusion

Using evolutionary crystal structure prediction, we have studied the Fe–S system at pressures from 100 GPa to 400 GPa, which encompasses the entire pressure range of the Earth's core. We found that only three compounds are stable — Fe_2S, FeS, and FeS_2 — and analyzed their crystal structures. We resolved the FeS conundrum, where the experimentally observed high-pressure high-temperature CsCl-type phase was not found to be stable in theory; here, we showed that this phase is thermally stabilized and does not have a stability field at zero temperature. We showed that the predicted high-pressure *Pmmn* phase of FeS is structurally related to well-known mackinawite and can be easily obtained by compression of mackinawite.

Among the predicted compounds only Fe_2S may exist in the Earth's inner core in equilibrium with excess Fe. We

determined the amounts of S, Si, and O needed to explain the observed density of the inner core, and found them to be around 12, 10, and 16 mol.%, respectively (assuming only one light alloying element). Taking into account also the mean atomic mass $\bar{M}$, we arrived at four plausible compositional models of the inner core (in atomic %):

(a) 86%(Fe + Ni) + 14%C,
(b) 84%(Fe + Ni) + 16%O,
(c) 84%(Fe + Ni) + 7%S + 9%H,
(d) 85%(Fe + Ni) + 6%Si + 9%H.

Linear combinations of models (c) and (d), and perhaps (a) and (b), are also possible. From previous experiments [70–72], it is known that model (a) not only explains the density and average atomic mass in the inner core, but seismic wave velocities and the anomalous Poisson ratio of the inner core, as well. Models (b–d) remain to be tested against these constraints, and all models need to be checked for compatibility with constraints imposed on the liquid outer core.

Acknowledgments

Calculations were performed at the Supercomputing Center of Lomonosov Moscow State University, and on Rurik supercomputer of our laboratory at MIPT. We thank the Russian Science Foundation (grant 16-13-10459) for financial support.

References

1. Birch F *J. Geophys. Res.* **69** 4377 (1964)
2. Birch F *J. Geophys. Res.* **57** 227 (1952)
3. Poirier J-P *Introduction to the Physics of the Earth's Interior* 2nd ed. (Cambridge: Cambridge Univ. Press, 2000)
4. Bazhanova Z G, Oganov A R, Gianola O *Phys. Usp.* **55** 489 (2012); *Usp. Fiz. Nauk* **182** 521 (2012)
5. Li J et al. *Earth Planet. Sci. Lett.* **193** 509 (2001)
6. Chen B et al. *Proc. Natl. Acad. Sci. USA* **104** 9162 (2007)
7. Alfè D, Gillan M J, Price G D *Earth Planet. Sci. Lett.* **195** 91 (2002)
8. Badro J, Côté A S, Brodholt J P *Proc. Natl. Acad. Sci. USA* **111** 7542 (2014)
9. Hirose K, Labrosse S, Hernlund J *Annu. Rev. Earth Planet. Sci.* **41** 657 (2013)
10. Saxena S, Eriksson G *Calphad* **51** 202 (2015)
11. Akahama Y, Kobayashi M, Kawamura H *Phys. Rev. B* **48** 6862 (1993)
12. Luo H, Greene R G, Ruoff A L *Phys. Rev. Lett.* **71** 2943 (1993)
13. Degtyareva O et al. *High Pressure Res.* **25** 17 (2005)
14. Zakharov O, Cohen M L *Phys. Rev. B* **52** 12572 (1995)
15. Rudin S P, Liu A Y *Phys. Rev. Lett.* **83** 3049 (1999)
16. Mao H-K, Bassett W A, Takahashi T *J. Appl. Phys.* **38** 272 (1967)
17. Vočadlo L et al. *Phys. Earth Planet. Inter.* **117** 123 (2000)
18. Steinle-Neumann G, Stixrude L, Cohen R E *Proc. Natl. Acad. Sci. USA* **101** 33 (2004)
19. Saxena S K, Dubrovinsky L S, Häggkvist P *Geophys. Res. Lett.* **23** 2441 (1996)
20. Andrault D et al. *Science* **278** 831 (1997)
21. Belonoshko A B, Ahuja R, Johansson B *Nature* **424** 1032 (2003)
22. Belonoshko A B et al. *Phys. Rev. B* **74** 214102 (2006)
23. Gorbatov O I et al. *J. Nucl. Mater.* **419** 248 (2011)
24. Stixrude L, Cohen R E *Geophys. Res. Lett.* **22** 125 (1995)
25. Vočadlo L et al. *Nature* **424** 536 (2003)
26. Dubrovinsky L et al. *Science* **316** 1880 (2007)
27. Kuwayama Y et al. *Earth Planet. Sci. Lett.* **273** 379 (2008)
28. Tateno S et al. *Science* **330** 359 (2010)
29. Côté A S, Vočadlo L, Brodholt J P *Earth Planet. Sci. Lett.* **345 – 348** 126 (2012)
30. Ono S et al. *Earth Planet. Sci. Lett.* **272** 481 (2008)
31. Sata N et al. *Am. Mineral.* **93** 492 (2008)
32. Oganov A R, Glass C W *J. Chem. Phys.* **124** 244704 (2006)
33. Oganov A R, Lyakhov A O, Valle M *Acc. Chem. Res.* **44** 227 (2011)
34. Lyakhov A O et al. *Comput. Phys. Commun.* **184** 1172 (2013)
35. Hohenberg P, Kohn W *Phys. Rev.* **136** B864 (1964)
36. Kohn W, Sham L J *Phys. Rev.* **140** A1133 (1965)
37. Perdew J P, Burke K, Ernzerhof M *Phys. Rev. Lett.* **77** 3865 (1996)
38. Dewaele A et al. *Phys. Rev. Lett.* **97** 215504 (2006)
39. Dubrovinsky L S et al. *Phys. Rev. Lett.* **84** 1720 (2000)
40. Mao H K et al. *J. Geophys. Res. Solid Earth* **95** 21737 (1990)
41. Jephcoat A P, Mao H K, Bell P M *J. Geophys. Res. Solid Earth* **91** 4677 (1986)
42. Ono S, Kikegawa T *Am. Mineral.* **91** 1941 (2006)
43. Blöchl P E *Phys. Rev. B* **50** 17953 (1994)
44. Kresse G, Joubert D *Phys. Rev. B* **59** 1758 (1999)
45. Kresse G, Furthmüller G *J. Phys. Rev. B* **54** 11169 (1996)
46. Methfessel M, Paxton A T *Phys. Rev. B* **40** 3616 (1989)
47. Blöchl P E , Jepsen O, Andersen O K *Phys. Rev. B* **49** 16223 (1994)
48. Dudarev S L et al. *Phys. Rev. B* **57** 1505 (1998)
49. Togo A, Oba F, Tanaka I *Phys. Rev. B* **78** 134106 (2008)
50. Togo A, Tanaka I *Scripta Mater.* **108** 1 (2015)
51. Birch F *Phys. Rev.* **71** 809 (1947)
52. Parthasarathy G *Geochim. Cosmochim. Acta A* **68** (Suppl. 11) 93 (2004)
53. Gudelli V K et al. *J. Phys. Chem. C* **117** 21120 (2013)
54. Lennie A R et al. *Mineral. Mag.* **59** 677 (1995)
55. Grimme S *J. Comput. Chem.* **27** 1787 (2006)
56. Tkatchenko A, Scheffler M *Phys. Rev. Lett.* **102** 073005 (2009)
57. Dion M et al. *Phys. Rev. Lett.* **92** 246401 (2004)
58. Román-Pérez G, Soler J M *Phys. Rev. Lett.* **103** 096102 (2009)
59. Klimeš J, Bowler D R, Michaelides A *J. Phys. Condens. Matter* **22** 022201 (2010)
60. Klimeš J, Bowler D R, Michaelides A *Phys. Rev. B* **83** 195131 (2011)
61. Thonhauser T et al. *Phys. Rev. B* **76** 125112 (2007)
62. Zhang F, Oganov A R *Geophys. Res. Lett.* **37** L02305 (2010)
63. Weerasinghe G L, Pickard C J, Needs R J *J. Phys. Condens. Matter* **27** 455501 (2015)
64. Dziewonski A M, Anderson D L *Phys. Earth Planet. Inter.* **25** 297 (1981)
65. Alfè D et al. *Philos. Trans. R. Soc. Lond. A* **360** 1227 (2002)
66. Huang H et al. *Nature* **479** 513 (2011)
67. Narygina O et al. *Earth Planet. Sci. Lett.* **307** 409 (2011)
68. Litasov K D, Shatskiy A F, Ohtani E *Geochem. Int.* **54** 914 (2016)
69. Hirose K et al. *Nature* **543** 99 (2017)
70. Prescher C et al. *Nature Geosci.* **8** 220 (2015)
71. Chen B et al. *Geophys. Res. Lett.* **39** L18301 (2012)
72. Chen B et al. *Proc. Natl. Acad. Sci. USA* **111** 17755 (2014)